Appl. Phys. B 80, 833–839 (2005)
DOI: 10.1007/s00340-005-1811-8

Applied Physics B
Lasers and Optics

B. SMEETS[1,] ✉
R.W. HERFST[1]
L.P. MAGUIRE[2]
E. TE SLIGTE[1]
P. VAN DER STRATEN[1]
H.C.W. BEIJERINCK[1]
K.A.H. VAN LEEUWEN[1]

Laser collimation of an Fe atomic beam on a leaky transition

[1]Eindhoven University of Technology, Department of Physics, P.O. Box 513, 5600MB Eindhoven, The Netherlands
[2]School of Physics, University of Melbourne, Victoria 3010, Australia

Received: 14 January 2005 /
Revised version: 11 March 2005
Published online: 9 May 2005 •

ABSTRACT We report results of the first laser collimation of a thermal beam of Fe atoms on the leaky $^5D_4 \rightarrow {}^5F_5$ transition, with both parallel linear $\pi^x\pi^x$ and crossed linear $\pi^x\pi^y$ laser polarization configurations. The measured atomic beam divergence is compared to a rate-equation model and a quantum Monte Carlo model. The experimental values for the divergence are limited by the finite laser line width, which is comparable to the natural line width of the Fe atom. In general, flux decreases with higher intensities, showing the effect of the leaky transition. At the best beam collimation $\alpha_{\mathrm{RMS}} = 0.17$ mrad, which is for a detuning of $\delta = -\Gamma$ and a saturation parameter of $s = 6$, the flux decreased to approximately 70%. Highest flux was measured for a detuning of $\delta = -2\Gamma$ and $s = 4$, reaching 135% of the uncooled value. From our measurements we estimate the total leak rate to be $1/(240 \pm 40)$, which is in good agreement with the literature value of 1/244. The crossed linear polarization configuration is the better choice, with a slightly better collimation but the same atomic beam flux. Plugging of the largest leak would increase the flux to at least 80% of the closed transition value, resulting in better contrast for atom lithography.

PACS 32.80.Lg; 32.80.Pj; 42.50.Vk

1 Introduction

Collimation of atomic beams by laser cooling has become an important technique in the preparation of experiments in various fields of atomic physics. An interesting application is atom lithography. The idea of atom lithography is the focusing of atoms by a standing light wave onto a substrate, which generates nanosized periodic structures with a perfect periodicity. This technique has been applied successfully to sodium [1], chromium [2, 3], aluminum [4], and ytterbium [5] beams. Recently, iron nanolines were also produced by atom lithography [6, 7], which opens the way to directly deposited ferromagnetic nanostructures.

In order to create the narrowest possible structures, the atomic beam should be collimated. Starting from an effusive beam source, collimation can be achieved mechanically by using two apertures. However, this straightforward technique results in a drastic loss of flux. Laser cooling provides a solution: by transverse cooling of the atomic beam, the collimation can be increased without flux loss. The basic idea of laser cooling is that atoms are cooled by the dissipative force arising from the interaction between the atoms and counter-propagating laser beams detuned below resonance. When both beams have identical polarization, the cooling is based on the Doppler effect. Cooling arises from the fact that atoms absorb more photons from the laser beam that propagates in the direction opposite to their own motion. This is often referred to as Doppler cooling. Two counter-propagating laser beams with orthogonal linear polarizations give rise to the so-called Sisyphus cooling. This can drastically increase the effectiveness of the cooling, reaching temperatures well below the limit of Doppler cooling. For a review of laser cooling, see Ref. [8].

We present the first laser collimation of an atomic Fe beam for use in atom lithography of ferromagnetic structures. Iron is the most accessible ferro-magnetic element for laser-focused deposition. The most practical transition of Fe for laser cooling is the 372.099-nm $^5D_4(3d^64s^2) \rightarrow {}^5F_5(3d^64s4p)$ transition, with a lifetime of 61.73 ns ($\Gamma = 2.58(2\pi)$ MHz), since it can be accessed by a frequency-doubled titanium:sapphire (Ti:S) laser. The use of this transition exhibits one problem; this transition is not closed. An excited Fe atom can spontaneously decay to three long-lived ($\tau > 1$ s) metastable states besides the ground state (Fig. 1). The total probability of decay to those states is 1/244 as given by the NIST manual [9]. Thus, on average after 244 spontaneous emissions, the atom will escape from the laser cooling cycle and will no longer interact with the light. A solution for leaky transitions are repumper lasers tuned to the wavelengths with the largest leak rates, which continuously transfer the leaked atoms back to the excited state, and hence back into the cooling cycle. The largest leak in Fe can be closed with light of $\lambda = 501$ nm, reducing the leak rate to 1/1400. At this moment, no compact commercially available laser produces this wavelength. For this purpose, a frequency-doubled Ti:S laser or diode laser tuned to 1002 nm can be used. Therefore, we have opted not to use a repumper laser. In this paper, we investigate what can be achieved with laser cooling in the presence of the leaks.

These leaks have two important consequences. First, laser cooling has to be achieved with a restricted number of photons.

✉ Fax: +31-40-245-60-50, E-mail: b.smeets@tue.nl

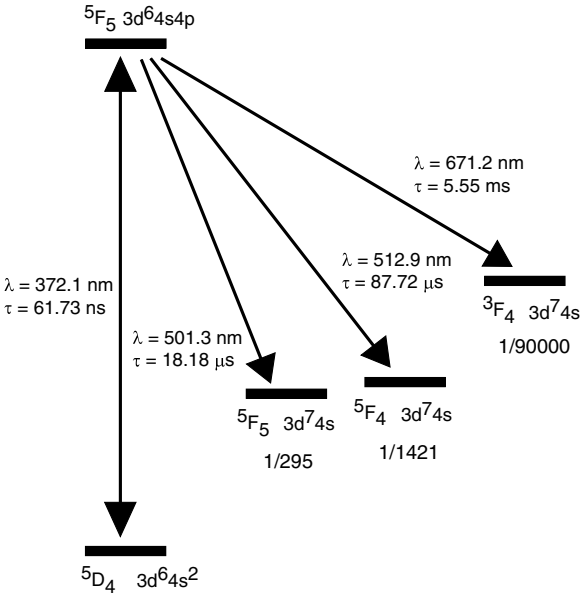

FIGURE 1 Energy-level diagram of the $^5D_4 \rightarrow {}^5F_5$ transition, including the three leaks to metastable states

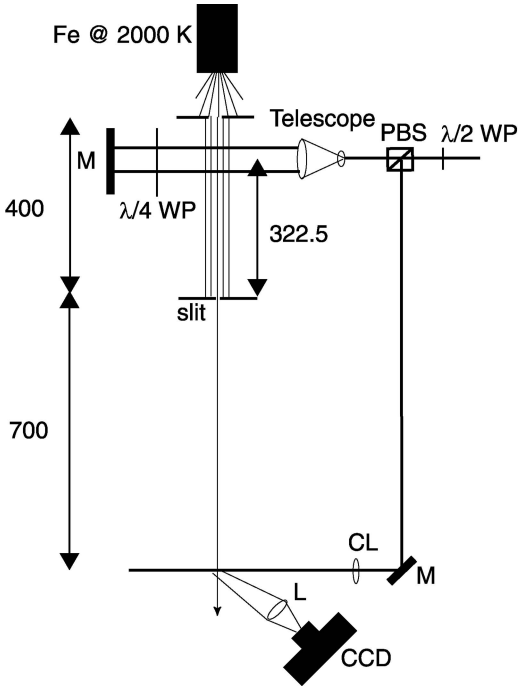

FIGURE 2 Schematic view of the setup. The Fe atoms that emerge from a crucible heated to 2000 K pass through a skimmer of 0.5-mm diameter and are laser cooled by a telescopically enlarged laser beam with a waist of 60 mm truncated to 45 mm in the longitudinal direction of the atomic beam, 50 mm downstream from the skimmer. A slit of 10 μm is placed in the atomic beam 400 mm downstream from the skimmer to measure the divergence of the atomic beam. A highly saturated probe beam excites the Fe atoms 700 mm downstream from the slit. The resulting fluorescence is imaged with a CCD camera, looking from the *top* in the figure, to obtain a spatial profile of the atomic beam

Therefore, cooling to the equilibrium temperature limit cannot be achieved. Second, a significant fraction of the atomic beam will leave the cooling region in a metastable state. These atoms are not focused by the standing light wave and contribute to a background flux that limits the contrast of the atomic beam focusing. In the case of Fe this would lead to a large ferromagnetic background layer, which prohibits the fabrication of separated nanomagnets.

In this paper we explore experimentally and theoretically one-dimensional laser collimation of an Fe atomic beam with both $\pi^x\pi^x$ (parallel linear polarization) and $\pi^x\pi^y$ (crossed linear polarization) laser beam configurations. In particular, we look at the obtained divergence of the atomic beam, and the effect of the leaky transition on the atomic beam flux for several laser intensities and detunings. Our results show that laser collimation on a leaky transition seriously decreases the useful flux compared to a closed-transition collimation. This will eventually lead to a thick uniform layer of Fe atoms of the same order of magnitude as the height of the laser-focused structures. A tradeoff between collimation, resulting in narrow structures, and useful flux, implying good structure to background ratio, should be made. In Sect. 2, the experimental setup is described. The simulation methods are explained in Sect. 3. Section 4 will deal with the results, followed by the conclusions in Sect. 5.

2 Experimental setup

In Fig. 2 a schematic view of the setup is given. The Fe beam is produced using an Al_2O_3 crucible with an orifice of 1 mm heated by a carbon spiral heater [10]. The operating temperature of the source is typically 2000 K. At that temperature, the Knudsen number is $K_n = 4$; thus, a Maxwell–Boltzmann distribution can be assumed. The average longitudinal velocity of the Fe atoms is $(8k_BT/\pi M)^{1/2} = 870$ m/s. The Fe beam intensity is typically $I_{Fe} = 2.5 \times 10^{16}$ s^{-1} sr^{-1}. This value is almost a factor of 10 lower than in the setup used in Ref. [7], where the source is operated at 2150 K. However, for the present series of measurements the absolute value of the beam intensity is of less importance than for deposition experiments. The atomic beam is further defined by a 0.5-mm-diameter skimmer, 150 mm downstream from the nozzle. The isotope ^{56}Fe has a natural abundance of 91.8%, of which at a temperature of 2000 K some 50% is still in the $^5D_4$ ground state. Hyperfine structure is absent in ^{56}Fe, since the nuclear spin is zero.

The 372-nm light is generated by a frequency-doubled Ti:S laser (Coherent 899-21), pumped by an Ar-ion laser (Coherent Innova 200). This laser is locked to the $^5D_4 \rightarrow {}^5F_5$ transition by polarization spectroscopy on an Fe–Ar hollow-cathode discharge within 0.2 MHz [11], as determined from the error signal. However, this signal is filtered by a lock-in amplifier with an output time constant of 100 ms. Therefore, all components of the laser FM noise above 1.6 Hz will not be included in this figure and the actual FM noise will be larger than 0.2 MHz. We estimate the laser line width of our UV laser to be around 1 MHz RMS, based on the specifications of the Ti:S laser. This is close to half the natural line width of the $^5D_4 \rightarrow {}^5F_5$ transition.

Laser cooling is performed 50 mm downstream from the skimmer. For laser cooling a Gaussian laser beam with a waist ($1/e^2$ radius) of 60 mm is truncated to an interaction region of 45 mm along the atom beam. Therefore, the intensity of the

laser beam decreases by 30% at the edges of the interaction region in the longitudinal direction. Transversely to the atomic beam, the laser beam has a waist of 0.75 mm, creating an interaction region in which the intensity decreases by 10% at the edges of the atomic beam. A quarter-wave plate is placed in front of the back-reflecting mirror, in order to create the $\pi^x\pi^y$ polarization configuration.

The atoms are detected 1.1 m downstream from the skimmer by light-induced fluorescence. The fluorescence resulting from a highly saturated probe beam is imaged by a CCD (Apogee 47P) camera. In order to reduce the focal depth, the probe beam is focused to a directed light sheet with waists of 50 μm and 1 mm perpendicular to and in the axial direction of the atomic beam, respectively. The magnification of our imaging setup is 1/1.45. The pixel size of our CCD camera is 10 μm, resulting in an imaging resolution of 7 μm.

The divergence of the laser-cooled atomic beam is measured by means of a 10-μm slit placed 400 mm downstream from the skimmer. The fact that the slit is positioned a certain distance from the skimmer imposes an upper limit on the measurable divergence. The maximum divergence that can be measured is calculated from the size of the atomic beam after the laser-cooling section, which is approximately equal to the size of the skimmer (0.5 mm), and the distance from the center of the laser-cooling section to the slit (322.5 mm). This limits the maximum measurable divergence to approximately 0.35 mrad RMS. The angular resolution of our detection system is 0.01 mrad.

In Fig. 3 a typical measurement is shown. The image captured with the CCD camera was line averaged over the size of the probe laser beam in the axial direction of the atomic beam. The uncooled atomic beam is compared with an example of a laser-cooled atomic beam, with saturation parameter $s = I/I_0 = 4$, saturation intensity $I_0 = 62\ \mu\text{W/mm}^2$, and laser detuning $\delta = -\Gamma$ for the $\pi^x\pi^y$ configuration.

3 Simulations

To investigate the role of the leaky transition, we have simulated the collimation experiment using two different models; a rate-equation (RE) model and a quantum Monte Carlo (QMC) model. Here, we briefly describe these models.

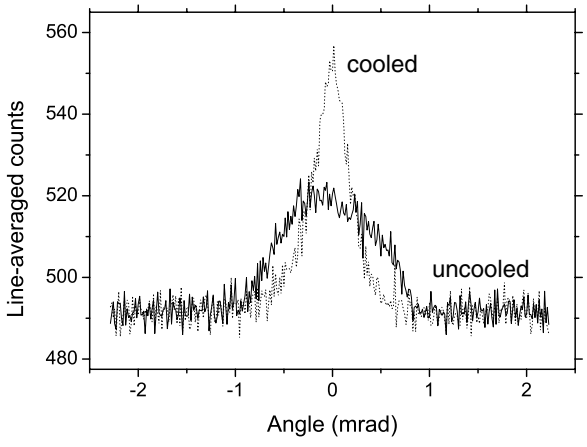

FIGURE 3 Example of an angular distribution image with an exposure time of the CCD camera of 10 s. One image is captured without laser-cooling beams (*straight line*) and the other with laser cooling (*dotted line*), with a saturation parameter of $s = I/I_0 = 4$ and a detuning $\delta = -\Gamma$ for the $\pi^x\pi^y$ configuration. The width of the uncooled beam is geometrically limited to 0.35 mrad RMS

3.1 *Rate-equation (RE) model*

This program keeps track of all the velocity changes due to absorptions and spontaneous emissions of photons. The actual absorption from a particular laser beam is determined by a Monte Carlo method based on the rate of absorption for each laser beam [12]:

$$R = \frac{s\Gamma}{2(1 + s + (2\delta/\Gamma)^2)}, \tag{1}$$

with Γ the natural line width of the specific atomic species, s the saturation parameter which is given by the ratio of the laser intensity I to the saturation intensity I_0 of the particular transition, and $\delta = \omega_l - \omega_{eg}$ the detuning from the resonance frequency. Absorption of photons will be in the direction of the laser beam $\hat{k}$; in contrast, spontaneous emission will occur in a random direction according to the dipole radiation distribution. This leads to a net momentum transfer into the direction of the laser beam, resulting in a force

$$\mathbf{F} = R\hbar\mathbf{k}. \tag{2}$$

An atom moving with a velocity $\mathbf{v}$ is Doppler shifted with $-\mathbf{k}\cdot\mathbf{v}$, obtaining an effective detuning of $\delta_{\text{eff}} = \delta - \mathbf{k}\cdot\mathbf{v}$. Cooling occurs when an atom is irradiated by two identical laser fields with opposite directions $\pm\hat{k}$. The magnitude of the resulting force is then $F = -\beta v_\perp$, with β the damping coefficient and $v_\perp = \hat{k}\cdot\mathbf{v}$ the velocity of the atom parallel to the laser beams.

The simulation proceeds as follows: at each point of the trajectory of the atom, the absorption rate from the specific ground-state magnetic sublevel of the atom at that point is calculated. Then, a small time interval $\mathrm{d}t$ is chosen such that the probability of absorbing a photon $\mathrm{d}P$ is small. A random pick from a Poisson distribution with average $\mathrm{d}P$ decides how many photons are absorbed. Normally this number is zero, but there is a small chance that one photon is absorbed in the time interval $\mathrm{d}t$. The velocity of the atom is changed, according to the recoil momentum of the absorbed photon. The atom is now in the excited state and will spontaneously decay back to the ground state. Which magnetic substate of the ground state the atom ends up in depends on the square of the Clebsch–Gordan coefficient for emitting a photon with a particular polarization. A random pick, weighted accordingly, will decide to which sublevel of the ground state the atom will decay. The atom will now move unperturbed during a time interval $\mathrm{d}t$, independent of whether a photon was absorbed or not. At this point, the process starts over again.

The program computes, for each laser intensity and detuning, 5000 atomic trajectories, with a Maxwell–Boltzmann longitudinal velocity distribution, which scales as $v^3\exp(-mv^2/2kT)$ conforming to the temperature of the Fe source. The experimental geometry is taken into account. The initial transverse velocity for each atom is randomly chosen in a range of −6 m/s to 6 m/s. This range is chosen to be wider

than the capture range of the cooling force (as they are the only atoms to be affected) but not so wide as to lead to excessive computation time. For atoms in the excited state, an extra decay channel is introduced with a total probability of 1/244 representing the leak channel. After decay, these atoms do not interact with the light field and follow their paths with a constant velocity.

3.2 *Quantum Monte Carlo (QMC) model*

The quantum Monte Carlo (QMC) model is based on Mollow's treatment of resonant light scattering [13]. A detailed description of the model for arbitrary light fields is given by Dum et al. [14]. What follows is a summary of the important features. In contrast with the other simulation models, the kinetic energy is included in the Hamiltonian, which implies that the wave function describes not only the internal states of the atom but also its center-of-mass motion. For an atom in a light field, the total Hamiltonian $\hat{H}$ is given by

$$\hat{H} = \frac{\hat{p}^2}{2M} + \hat{H}_{0\mathrm{A}} + \hat{H}_{0\mathrm{F}} + \hat{H}_{\mathrm{I}}(t), \tag{3}$$

with $\hat{p}$ the momentum of the atom and M the mass. The operator $\hat{H}_{0\mathrm{A}} = \hbar\omega_{\mathrm{eg}}\hat{a}^\dagger\hat{a}$ is the Hamiltonian of the free atom with $\hat{a} = |g\rangle\langle e|$ and $\hat{a}^\dagger = |e\rangle\langle g|$ the atomic lowering and raising operators, respectively. The kets $|g\rangle$ and $|e\rangle$ are the time-independent ground and excited states, respectively. The operator $\hat{H}_{0\mathrm{F}}$ represents the Hamiltonian of the free radiation field. In the dipole approximation the interaction Hamiltonian $\hat{H}_{\mathrm{I}}$ is given by

$$\hat{H}_{\mathrm{I}}(t) = -\mu^*_{\mathrm{eg}} \cdot \hat{\mathbf{E}}^\dagger\hat{a} + \mathrm{H.C.}, \tag{4}$$

with μ_{eg} the atomic dipole matrix and $\hat{E}$ the electric field operator. Mollow showed that a single-mode coherent light field can be treated classically when all the other modes of the light field are empty for $t \to -\infty$. Therefore, the light field can be represented by a complex vector $\varepsilon_{\mathrm{c}}(\mathbf{r}, t)$, which is for a plane wave in the z direction $\varepsilon_{\mathrm{c}}(z, t) = \varepsilon_0 \mathrm{e}^{\mathrm{i}(kz - \omega t)}$. At the start ($t = 0$) we assume that all light modes are empty, except for the laser mode. We split the wave function $\Psi(\mathbf{r}, t)$ into n partial wave functions $\Psi^n(\mathbf{r}, t)$, each with n spontaneously emitted photons:

$$\Psi(\mathbf{r}, t) = \Psi^0(\mathbf{r}, t) + \sum_{n=1}^{\infty} \Psi^n(\mathbf{r}, t). \tag{5}$$

For the partial wave function $\Psi^0(\mathbf{r}, t) = C^0_{\mathrm{g}}(\mathbf{r}, t)|g, \{0\}\rangle + C^0_{\mathrm{e}}(\mathbf{r}, t)|e, \{0\}\rangle$ a set of Schrödinger-like equations can be derived. The modulus $|\Psi^0(t)|^2 = |C^0_{\mathrm{g}}(t)|^2 + |C^0_{\mathrm{e}}(t)|^2$ is the probability that no spontaneous emissions have occurred until time t. The loss of probability $1 - |\Psi^0(t)|^2$ is equal to the photon waiting-time distribution $W(t)$, which is given by

$$1 - |\Psi^0(t)|^2 = \int_0^t W(t')\mathrm{d}t' = \Gamma \int_0^t |C^0_{\mathrm{e}}(t')|^2 \mathrm{d}t'. \tag{6}$$

In a Monte Carlo simulation this photon waiting-time distribution can be used to calculate the time at which a photon is spontaneously emitted by picking a random number $\Upsilon \in [0...1]$ and solving the equation

$$1 - |\Psi^0(t)|^2 = \Upsilon. \tag{7}$$

At this moment, we assume no further interaction with the spontaneously emitted photon, and start over in the zero-photon ground state with $C^0_{\mathrm{g}} = 1$ and all other C's zero. In the case of a two-level atom in a running wave laser field, the complete time evolution of the coefficients C^0_{g} and C^0_{e} is given by Mollow [13]; it has been applied to a Monte Carlo simulation of cooling processes [15, 16, 17] and generalized by Dum et al. [14] and Dalibard et al. [18] to an arbitrary light field and magnetic atomic substructure.

The momentum in the direction of the laser field is treated quantum mechanically with operator $\hat{p}$ and eigenstates $|p\rangle$. The motion perpendicular to the laser fields is treated classically. To include magnetic substructure, the partial wave functions Ψ^0 can be expanded in time-independent states $|\alpha, m_\alpha\rangle$ with coefficients $C_{\alpha \mathrm{m}_\alpha}$ ($\alpha = e,\ g$). The product wave function is represented by $|\alpha, m_\alpha, p\rangle$. If there is no spontaneous emission, the atomic momentum is quantized as $|p_0 + j\hbar k\rangle$ with $p_0 = \hbar k_0$ the initial momentum and j an integer number. We now have a family F_{p_0} of states that are internally coupled only by stimulated processes. The states of this family are denoted by $|\alpha, m_\alpha, j\rangle$ and have coefficients $C^j_{\alpha \mathrm{m}_\alpha}$. The momentum eigenvalues are $p_0 + j\hbar k$ with j even or odd for the ground states or excited states, respectively. Spontaneous emission will transfer an atom to another family $F_{\mathrm{p}'_0}$.

The equations of motion for the coefficients $C^j_{\alpha \mathrm{m}_\alpha}(t)$ for a family with initial momentum $p_0 = \hbar k_0$ are in a one-dimensional laser configuration in the z direction given by

$$\begin{aligned}
\mathrm{i}\hbar \frac{\mathrm{d}}{\mathrm{d}t} C^j_{\mathrm{gm_g}}(t) = {} & \left[\frac{\hbar^2}{2M}(jk + k_0)^2\right] C^j_{\mathrm{gm_g}}(t) \\
& + \frac{\hbar\Omega^*_{\mathrm{eg}}}{2} \langle j_{\mathrm{g}} m_{\mathrm{g}} 1 1 | j_{\mathrm{e}}(m_{\mathrm{g}} - 1)\rangle \left[\epsilon_1^{+*} C^{j+1}_{\mathrm{e}(m_{\mathrm{g}}-1)}(t) \right. \\
& \left. + \epsilon_1^{-*} C^{j-1}_{\mathrm{e}(m_{\mathrm{g}}-1)}(t)\right] \\
& + \frac{\hbar\Omega^*_{\mathrm{eg}}}{2} \langle j_{\mathrm{g}} m_{\mathrm{g}} 1 {-1} | j_{\mathrm{e}}(m_{\mathrm{g}}+1)\rangle \left[\epsilon_{-1}^{+*} C^{j+1}_{\mathrm{e}(m_{\mathrm{g}}+1)}(t) \right. \\
& \left. + \epsilon_{-1}^{-*} C^{j-1}_{\mathrm{e}(m_{\mathrm{g}}+1)}(t)\right],
\end{aligned} \tag{8}$$

$$\begin{aligned}
\mathrm{i}\hbar \frac{\mathrm{d}}{\mathrm{d}t} C^j_{\mathrm{em_e}}(t) = {} & \left[\frac{\hbar^2}{2M}(jk + k_0)^2 - \hbar(\Delta + \mathrm{i}\Gamma/2)\right] C^j_{\mathrm{em_e}}(t) \\
& + \frac{\hbar\Omega_{\mathrm{eg}}}{2} \langle j_{\mathrm{g}}(m_{\mathrm{e}} + 1) 1 1 | j_{\mathrm{e}}(m_{\mathrm{e}})\rangle \left[\epsilon_1^{+} C^{j-1}_{\mathrm{g}(m_{\mathrm{e}}+1)}(t) \right. \\
& \left. + \epsilon_1^{-} C^{j+1}_{\mathrm{g}(m_{\mathrm{e}}+1)}(t)\right] \\
& + \frac{\hbar\Omega_{\mathrm{eg}}}{2} \langle j_{\mathrm{g}}(m_{\mathrm{e}} - 1) 1 {-1} | j_{\mathrm{e}}(m_{\mathrm{e}})\rangle \left[\epsilon_{-1}^{+} C^{j-1}_{\mathrm{g}(m_{\mathrm{e}}-1)}(t) \right. \\
& \left. + \epsilon_{-1}^{-} C^{j+1}_{\mathrm{g}(m_{\mathrm{e}}-1)}(t)\right].
\end{aligned} \tag{9}$$

The Rabi frequency is $\Omega_{\mathrm{eg}} = \Gamma_{\mathrm{eg}}\sqrt{I/(2I_0)}$ with I_0 the saturation intensity. The relative strengths of the orthogonal circular polarization components $+1$ and -1 of the individual laser beams in the $+$ and $-$ directions are denoted by $\epsilon_{\pm 1^\pm}$.

For simulation of the experiment, a transverse momentum range from -80 to $+80\hbar k$ ($80\hbar k = 1.5$ m/s) is chosen, limited by the computation time since it is quadratic in the momentum range. For each laser intensity and detuning we simulate 1000 atoms each starting out as a plane atomic wave and thus with a single velocity. The interaction time is divided into small intervals. For simplicity the interaction time is fixed, assuming a single longitudinal velocity equal to the average longitudinal velocity corresponding to the temperature in the Fe source. This assumption does not result in significant differences compared to the situation of a Maxwell–Boltzmann distribution. This was checked by running the program for different interaction times and averaging the resulting momentum distributions, weighted according to a Maxwell–Boltzmann distribution. Each time a spontaneous emission takes place, the excited atom can decay to a metastable state with a probability of $1/244$. The simulation only follows the atoms in momentum space, neglecting information about experimental geometry.

3.3 *Implementation*

Both simulations are performed with a monochromatic light field. However, experimentally, the laser line width is of the same order as the natural line width of Fe. This is included in the simulations by assuming a Gaussian laser line width, with an RMS width of $\Gamma/2$. For each laser intensity, the RMS divergence of the atomic beam was quadratically averaged for five detunings, each weighted according to the Gaussian line-width distribution. The calculated RMS atomic beam divergence was masked with a Gaussian transmission function with an RMS divergence of 0.35 mrad, this being the geometrical limit of the experimental setup. In Fig. 4, the effect of the averaging on the resulting divergence of the atomic beam is visible for an average detuning of $\delta = -\Gamma/2$ as a function of laser intensity. From the large difference in the divergence obtained with the RE model and the QMC model for high intensities, it is clear that the RE model does not include all stimulated diffusion effects of atom–laser interactions. As can be seen from the QMC results, the contribution of the sub-Doppler cooling force is small due to the small capture range of this force in the case of Fe. This is a known effect for atoms with a small natural line width in combination with a large recoil velocity [19]. The discrepancy between the averaged and the monochromatic results is largest at low intensities: the atomic beam has a larger divergence for the other laser detunings included in the laser line width resulting in a larger average divergence. For high intensities, the difference is smaller, since cooling is efficient over a larger detuning range. The striking difference between the RE model and the QMC model for high intensity in the monochromatic case is almost entirely absent in the averaged results.

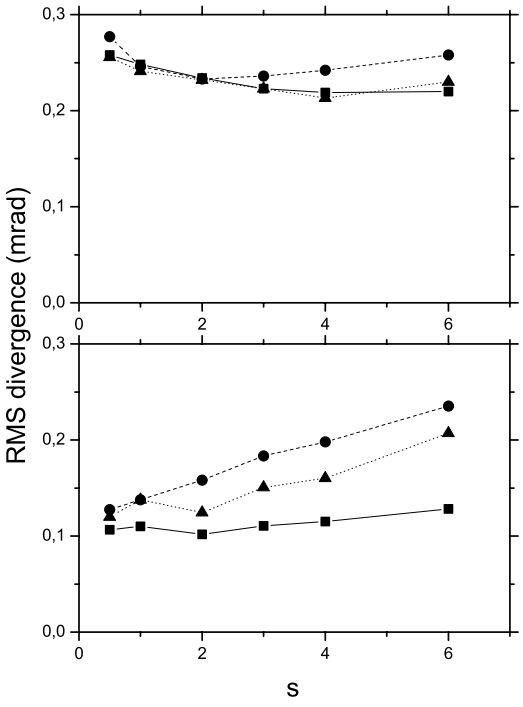

FIGURE 4 The effect of the averaging of five detunings on the simulated divergence of the atomic beam for an average detuning of $\delta = -1/2\Gamma$ as a function of laser intensity. The *squares* are results obtained with the RE model in the $\pi^x\pi^x$ polarization configuration. The *circles* and *triangles* are QMC simulations with a $\pi^x\pi^x$ and a $\pi^x\pi^y$ polarization configuration, respectively. In the *upper graph*, the atomic beam divergence convoluted with the laser line width is shown. In the *lower graph*, the simulated atomic beam divergence with a monochromatic light field is shown

4 Results and discussion

The atomic beam divergence was measured for a $\pi^x\pi^x$ and a $\pi^x\pi^y$ polarization configuration, for saturation parameters ranging from $s = 1/2$ to $s = 6$, and for three detunings: $\delta = -\Gamma/2$, $\delta = -\Gamma$, and $\delta = -2\Gamma$. These measurements are compared to the results from the simulation models.

In Fig. 5 the atomic beam divergences obtained from measurements and simulations are shown. The left-hand column shows results for the $\pi^x\pi^x$ configuration. The experimental error bars are of the order of the symbol size. Despite the rather crude implementation of the laser line width, the agreement between measurement and simulation is satisfying, implying that the cooling is mainly limited laser to a natural line-width ratio of ≈ 1. For a detuning of $\delta = -2\Gamma$ the measured atomic beam divergence is consistently lower than the simulated data. This could be attributed to a slight overestimation of the detuning in the experiment. The lower beam divergence simulated with the QMC model compared to the RE model for the $\delta = -2\Gamma$ case is due to the narrow momentum range over which the QMC program simulates, resulting in a smaller momentum range than the cooling force capture range. In the RE simulation atoms are also captured from outside the capture range of the cooling force. These atoms are not as cold, resulting in a larger atomic beam divergence. In the right-hand column, results for the $\pi^x\pi^y$ configuration are shown. This time, only QMC results are included, since the RE model cannot simulate this configuration. We achieved best collimation at an (average) detuning of $\delta = -\Gamma$ in the $\pi^x\pi^y$ configuration: $\alpha_{\mathrm{RMS}} = 0.17$ mrad.

In Fig. 6 the measured relative fluxes of ground-state Fe atoms through the 10-μm slit are shown and compared to the RE model. This flux measurement shows the effect of the

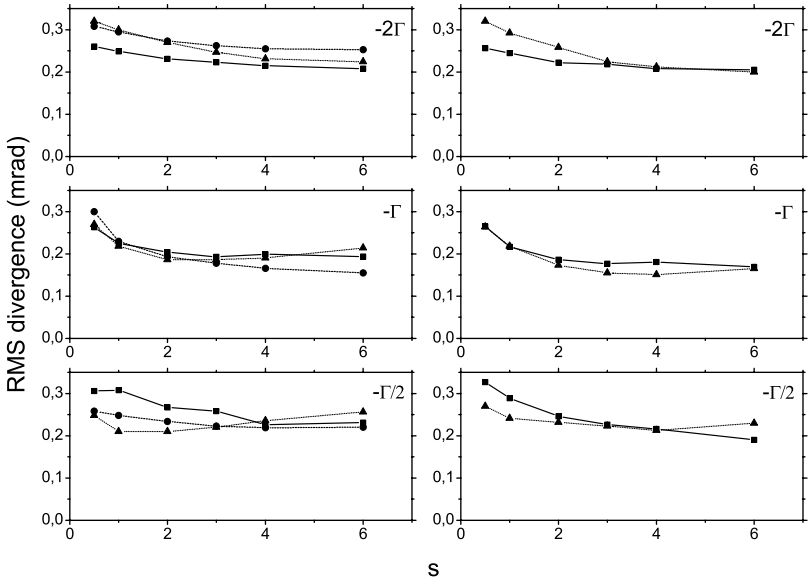

FIGURE 5 The atomic divergence obtained from measurements and simulations. In the *left-hand column*, results for the $\pi^x\pi^x$ configuration are shown. The *squares* are the measurements, the *circles* the RE model, and the *triangles* the QMC model. In the *right-hand column*, results for the $\pi^x\pi^y$ configuration are shown

leaky transition and is useful for optimizing laser parameters, balancing flux and collimation. Since the RE model is the only model that follows the atomic trajectories in momentum space and in real space, the flux was calculated from the RE simulation by placing a virtual slit at the position of the 10-μm slit in the real experiment. To obtain acceptable statistics, this virtual slit was 250-μm wide instead of 10 μm. As the virtual slit is half the source size, this does not affect the relative flux gain. The effect of the laser line width was included by averaging the flux obtained from monochromatic simulations at five different detunings. The measured fluxes are in reasonable agreement with the simulated data. Both in measurements and simulations, the effect of the leak is clearly visible: for a closed transition there is always flux gain for negative detuning. In contrast, we lose up to 65% of our flux at high intensity and small detuning.

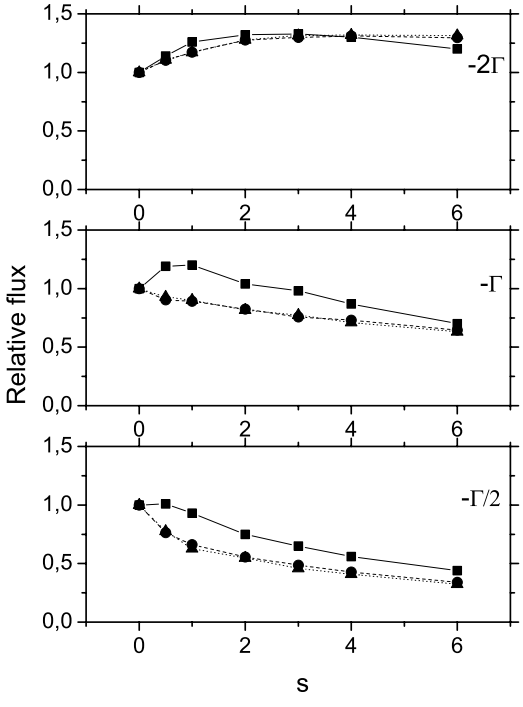

FIGURE 6 The measured relative fluxes through the 10-μm slit, compared to the rate-equation model. The *squares* are the RE simulations, the *circles* the measurements with the $\pi^x\pi^x$ polarization configuration, and the *triangles* the measurements with the $\pi^x\pi^y$ configuration. This flux measurement shows the effect of the leaky transition and is useful for optimizing laser parameters, balancing flux and collimation

Comparing the two laser polarization configurations, no significant difference was measured, meaning that the excited-state fraction during the interaction with the light is comparable in both cases. This gives the $\pi^x\pi^y$ configuration an advantage over the $\pi^x\pi^x$ case, since it collimates the atomic beam slightly better, without extra loss of flux. A large detuning is favorable, since flux gain is largest. In this case atoms are pushed into the relevant window due to the larger capture range of the cooling force, although this also implies a less efficient atomic beam collimation. A small detuning $\delta = -\Gamma/2$, the optimal value for Doppler cooling with monochromatic light and no leak channel, is not an optimal choice; the flux is lowest and collimation of the atomic beam is not optimal. The best beam collimation ($\alpha_{\mathrm{RMS}} = 0.17$ mrad) is reached for $\delta = -\Gamma$ and $s = 6$ in the $\pi^x\pi^y$ configuration. At these settings the flux decreases to 70% of the value without laser cooling. Highest flux gain is reached for a detuning of $\delta = -2\Gamma$: up to 135% of the non-cooled value.

To estimate the measured leak rate, we performed simulations at different leak rates. We compared these results with the measured fluxes for $s = 6$, since for high intensity the flux is less dependent on experimental parameters. This resulted in a leak rate of $1/(240 \pm 40)$, which is in agreement with the leak rate of 1/244 given in Ref. [9].

In Fig. 7 the relative fluxes obtained with the RE model for a monochromatic light field with and without leak channel are compared, for a detuning of $\delta = -\Gamma$. With increasing saturation parameter, the loss of flux due to the leak becomes even more pronounced, resulting in a loss of a factor of three at $s = 6$. The plugging of the largest leak with a 501-nm repumper results in a gain in flux up to a factor of approximately 2.5 at $s = 6$. The remaining flux loss is mainly due to decay

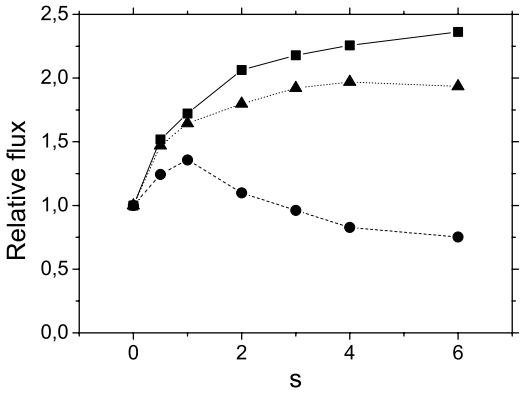

FIGURE 7 The relative flux for a detuning of $\delta = -\Gamma$ obtained with the RE model. The *squares* are flux values without leak channel. The *circles* are values with a leak rate of 1/244. The *triangles* represent the flux with the largest leak plugged

to the $^5F_4$ state with a leak rate of 1/1420. Decay to the $^3F_4$ state is too slow to have any significant effect on the flux. Assuming an excited-state fraction of 50% for high saturation parameters, a simple model $\exp(-t_{\rm int}/244\tau_{\rm eff}) = 0.18$, with $t_{\rm int} = (870/0.045)$ s the atom–light interaction time and $\tau_{\rm eff} = 2/\Gamma$ the effective absorption rate for high s, gives a lower limit of the ratio between fluxes with and without leak. For the data in Fig. 7 this ratio is 0.35 for high saturation intensity.

5 Conclusions

In conclusion, we have collimated a thermal beam of Fe atoms by laser cooling on a leaky transition. Both parallel linear ($\pi^x\pi^x$) and crossed linear ($\pi^x\pi^y$) laser polarization configurations are used. The experimental values for the atomic beam divergence are compared to a rate-equation model and a quantum Monte Carlo model. The collimation was limited by the finite laser line width, which was comparable to the natural line width of the Fe atom. In general, flux decreased with higher intensities, showing the effect of the leaky transition. A collimation of $\alpha_{\rm RMS} = 0.17$ mrad could be achieved; however, the flux decreased to approximately 70% of the non-cooled value. Highest flux was measured for a detuning of $\delta = -2\Gamma$, reaching 135% of the non-cooled value. The difference between both polarization configurations is small. The crossed linear polarization configuration gives the same flux, but slightly better collimation. Plugging of the largest leak would increase the flux to 80% of the closed-transition value for $s = 6$ or even higher for lower intensities, resulting in better contrast for atom lithography. From our measurements we estimate the leak rate to be $1/(240 \pm 40)$, which is in good agreement with a 1/244 leak rate found in the literature.

ACKNOWLEDGEMENTS This work is financially supported by the Dutch Foundation for Fundamental Research on Matter (FOM). The authors would like to thank E.J.D. Vredenbregt for his work on both simulation programs, and R.E. Scholten for lending his CCD camera for all the measurements included in this paper.

REFERENCES

1 G. Timp, R.E. Behringer, D.M. Tennant, J.E. Cunningham, Phys. Rev. Lett. **69**, 1636 (1992)
2 J.J. McClelland, R.E. Scholten, E.C. Palm, R.J. Celotta, Science **262**, 877 (1993)
3 U. Drodofsky, J. Stuhler, Th. Schulze, M. Drewsen, B. Brezger, T. Pfau, J. Mlynek, Appl. Phys. B: Photophys. Laser Chem. **65**, 755 (1997)
4 R.W. McGowan, D.M. Giltner, S.A. Lee, Opt. Lett. **20**, 2535 (1995)
5 R. Ohmukai, S. Urabe, M. Watanabe, Appl. Phys. B **77**, 415 (2003)
6 E. te Sligte, B. Smeets, K.M.R. van der Stam, R.W. Herfst, P. van der Straten, H.C.W. Beijerinck, K.A.H. van Leeuwen, Appl. Phys. Lett. **85**, 4493 (2004)
7 G. Myszkiewicz, J. Hohlfeld, A.J. Toonen, A.F. van Etteger, O.I. Shklyarevskii, W.L. Meerts, Th. Rasing, E. Jurdik, Appl. Phys. Lett. **85**, 3842 (2004)
8 H.J. Metcalf, P. van der Straten, *Laser Cooling and Trapping* (Springer, Berlin Heidelberg New York, 1999)
9 NIST Atomic Spectra Database, http://www.physics.nist.gov/cgi-bin/AtData/main/_asd
10 R.C.M. Bosch, H.C.W. Beijerinck, P. van der Straten, K.A.H. van Leeuwen, Eur. Phys. J.: Appl. Phys. **18**, 221 (2002). The atomic beam source described in this paper is used in thermal mode
11 B. Smeets, R.C.M. Bosch, P. van der Straten, E. te Sligte, R.E. Scholten, H.C.W. Beijerinck, K.A.H. van Leeuwen, Appl. Phys. B **76**, 815 (2003)
12 E.J.D. Vredenbregt, K.A.H. van Leeuwen, Am. J. Phys. **71**, 760 (2003)
13 B.R. Mollow, Phys. Rev. A **12**, 1919 (1975)
14 R. Dum, P. Zoller, H. Ritsch, Phys. Rev. A **45**, 4879 (1992)
15 R. Blatt, W. Ertmer, P. Zoller, J.L. Hall, Phys. Rev. A **34**, 3022 (1986)
16 M.D. Hoogerland, M.N.H. Wijnands, H.J. Senhorst, H.C.W. Beijerinck, K.A.H. van Leeuwen, Phys. Rev. Lett. **65**, 1559 (1990)
17 M.D. Hoogerland, H.F.P. de Bie, H.C.W. Beijerinck, E.J.D. Vredenbregt, K.A.H. van Leeuwen, P. van der Straten, H.J. Metcalf, Phys. Rev. A **54**, 3206 (1996)
18 J. Dalibard, Y. Castin, K. Mølmer, Phys. Rev. Lett. **68**, 580 (1992)
19 P.D. Lett, W.D. Phillips, S.L. Rolston, C.E. Tanner, R.N. Watts, C.I. Westbrook, J. Opt. Soc. Am. B **6**, 2084 (1989)